Materials Science-Poland, 41(3), 2023, pp. 140-158
http://www.materialsscience.pwr.wroc.pl/
DOI: 10.2478/msp-2023-0039

Fabrication of biomimetic anisotropic crescent-shaped microstructured surfaces by laser shock imprinting

Jie Ji, Kangnan Meng, Pin Li, Zongbao Shen*

School of Mechanical Engineering, Jiangsu University, Zhenjiang, China

The crescent-shaped microstructure bionic to the slip zone of the slippery zone of the carnivorous plant genus *Nepenthes* was fabricated on the surface of copper foil by laser shock imprinting (LSI). The microstructure of crescent-shaped grooves was initially fabricated on the surface of the micro-mold by etching, and then the microstructure was replicated on the surface of copper foil through plastic deformation under laser shock loading. Increasing the laser shock energy or the number of shocks can increase the degree of replication of the crescent-shaped microstructure, the height of the crescent-shaped microstructure, and the contact angle of water droplets on the surface. The wettability of the surface of the crescent microstructure is anisotropic and increases with an increase in offset distance. The anisotropy of the crescent-shaped microstructure causes the solid–liquid contact line in the direction of the bottom of the arc to become a long and approximately straight line. According to the rule that controlling LSI processing parameters can fabricate surfaces with different heights and wettability, a gradient wetting surface consisting of crescent-shaped microstructures was designed to achieve the directional spreading of droplets. By altering the distribution of crescent-shaped microstructures, a type-I flow channel with the ability to limit the spreading range of water droplets was fabricated.

Keywords: *laser shock imprinting, crescent-shaped microstructure, anisotropic wettability, directional spreading of droplet, limitation of droplet spread*

1. Introduction

Organisms have evolved to form structures with different functions to adapt to the natural environment and the study of their functional properties and bionic fabrication have become a hot topic in recent years [1–3]. The anisotropic microstructures on the surfaces of some plants and animals have anisotropic wettability and give them excellent functionality [4]. Periodic nanostripes on the wings of the butterfly provide directional wettability on the wing surface, preventing dust from accumulating on the extremities of the wings near the body during dusting [5]. Multilevel grooves and tiny papilla-like microstructures on the surface of rice leaves cause anisotropic hydrophobicity in rice leaves [6]. The duckbill-shaped sloping holes on the surface of the peristome of *Nepenthes* allow raindrops to be transported from inside the cage band to the outside, avoiding contamination of the digestive juices inside the cage by raindrops [7]. The three-dimensional ratchet structure of the *Araucaria* leaf, which is characterized by transverse and longitudinal reentrant curvature, allows low-surface-tension fluids to follow the inclined direction of the ratchet, while high-surface-tension fluids choose the opposite direction [8]. Inspired by natural phenomena, artificial anisotropic surfaces that imitate microstructures have the potential for significant applications in fluid control, water directional transport, etc. and have attracted a lot of attentions [9–11].

It was discovered that the slip function of the internal slip zone of the leaf cage of *Nepenthes* is closely correlated with the wettability of its crescent-shaped microstructure surface [12]. Consequently, the wettability of the surface of the crescent-shaped microstructure can be investigated via biofabrication. As a result of the asymmetry of the characteristic shape of the crescent-shaped microstructure in various directions, the surface of its characteristic array will also exhibit anisotropic wettability. Studying the fabrication of anisotropic micro and nanostructures on surfaces can be done through a variety of methods. Zhang

* E-mail: szb@ujs.edu.cn

© Jie Ji et al. 2023. This is an open access article distributed under the Creative Commons Attribution-NonCommercial-NoDerivatives 4.0 License. (http://creativecommons.org/licenses/by-nc-nd/4.0/)

et al. [13] fabricated a bionic peristome structure of *Nepenthes* using the template method and successfully achieved dynamic regulation of unidirectional water delivery under temperature control. Barraza et al. [14] successfully fabricated an anisotropic bionic rice leaf surface using the 3D printing method combined with TiO_2-HTMS layers. Bayindir et al. [15] fabricated large-area anisotropic hydrophobic polymer surfaces similar to the surface of rice leaves using a thermal drawing method. Yong et al. [16] similarly used a femtosecond laser to ablate stripe array structures with different spacing on the PDMS surface and systematically investigated the relationship between static and dynamic wettability along lines parallel and perpendicular to the stripe direction and the stripe period. Stafford et al. [17] fabricated microwrinkle characteristics with anisotropic wettability using the surface wrinkling technique. Compared with other processing methods, the laser shock imprinting (LSI) technology, as a surface microforming process, has been gradually applied to the field of microstructure processing in recent years, with higher processing accuracy, controllable cost, high processing efficiency, and stronger mechanical properties of its surface because it is obtained through plastic deformation [18, 19]. Jin et al. [20], successfully fabricated the surface profile of bamboo leaf blades on aluminum foil by LSI, which can improve the application of friction nanogenerators. Man et al. [21], successfully fabricated nanowire textures with excellent morphology on aluminum foil using a LSI process and investigated the effects of pulsed laser energy and laser pretreatment on the fabrication of nanowire textures. Yang et al. [22] used LSI to fabricate high-precision complex microwoven structures, and the forming accuracy of the microstructure was measured by filling rate and perpendicularity, which enabled high-precision formation of microwoven structures. Kim et al. [23] effectively fabricated a microscale pattern array on an aluminum surface using LSI and investigated various pressure transfer schemes of the laser shock waves in the laser shock micro-patterning process, as well as the effect of the use of an ablation layer on the micro-patterning performance. Yang et al. [24] used temperature-assisted LSI for better forming height, quality, and high-temperature stability. Yang et al. [25] fabricated the high-quality micro-pattern on laser pre-shocked aluminum foil by LSI.

In this paper, LSI was used to fabricate biomimetic crescent-shaped microstructures on the surface of copper foil to study the forming laws of crescent-shaped microstructures on workpiece surfaces and anisotropic wettability. The influence of LSI-processing parameters on the formation morphology, height, and wettability of crescent-shaped microstructures on the surface of copper foil was investigated. The influence of different offset distances of crescent-shaped microstructures on the anisotropic wettability of the surface of the workpiece was investigated. And its structure and wettability anisotropy were exploited. A liquid-gradient wettable surface consisting of crescent-shaped microstructures was designed for the realization of droplet directional spreading, which is achieved by fabricating different wettability zones with different LSI-processing parameters and lapping them to generate the wettability gradient. By altering the distribution position of the crescent-shaped microstructure on the surface of the workpiece, a flow channel was designed and fabricated to limit the spreading range of liquid droplets.

2. Experimental principles and methods

2.1. Method of fabrication of micro-molds

The design of the crescent-shaped microstructure was inspired by the biological structural characteristics of the surface of the internal slip zone of the *Nepenthes* leaf cage [12, 26]. The main parameters of the fabricated crescent-shaped microstructure unit on the surface of the mold are shown in Fig. 1(a), which consists of two circular arcs, R_1 and R_2, surrounded by two circular arcs: R_3 with the same radius tangent, where the distance between the two circles is L. The parameters of the crescent-shaped microstructure characteristic array are shown in Fig. 1(b), where X_0 is the spacing of adjacent crescents in the peer group, Y_0 is

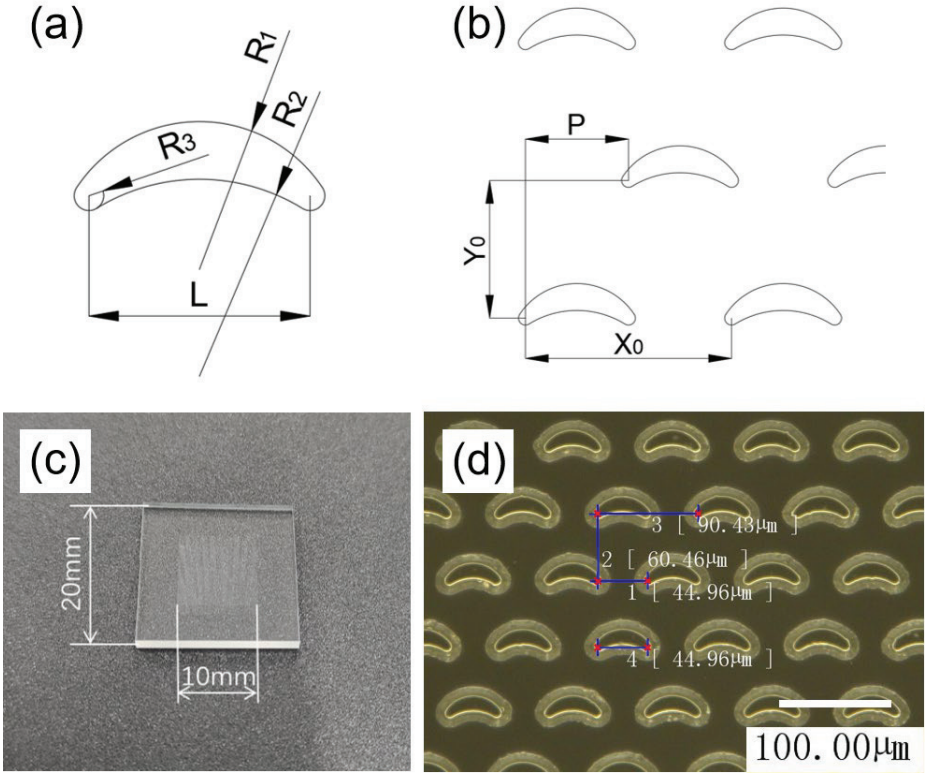


Fig. 1. Bionic crescent-shaped microstructure mold: (a) parameters of microstructure characteristics on the mold surface; (b) parameters of the crescent-shaped microstructure array on the mold surface; (c) physical mold; and (d) the physical surface structure of the mold

the spacing of adjacent rows, and P is the offset distance between adjacent rows.

In this investigation, the surface of the glass mold was selectively removed by the etching method. The specific plan was as follows: On the cleansed glass material, an adhesive (positive photoresist, AZ1500) was applied and then dried. The mask master was covered with the ;urface, and it was exposed to UV light (H94-30,SVC). The light-transmitting part of the photoresist protective layer on its surface was removed. The this part removed was the crescent-shaped microstructure required by the study. It was then cleaned and dried. The light-transmitting part of the adhesive protective layer was etched with hydrofluoric acid plus ammonium fluoride buffer solution (ratio 1:7), and the time required for corrosion was approximately 2 hours. The material was taken out of the solution and cleaned. The material was placed in a 100? thermostatic oven for 30 minutes so that the adhesive protective layer formed a firm film. The adhesive protective layer and coating layer were removed with alcohol. The mold was cut into the required single-piece size by the scribing machine.

Table 1. Parameters of the fabricated molds

Mold type	P (μm)	L (μm)	R_1 (μm)	R_2 (μm)	R_3 (μm)	X_0 (μm)	Y_0 (μm)
Mold 1	0						
Mold 2	30	45	30	36	4	90	60
Mold 3	45						

The three molds fabricated are shown in Table 1. Taking mold 3 as an example, the fabricated 20 mm $\times$ 20 mm $\times$ 2 mm glass mold is shown in Fig. 1(c), with a 10 mm $\times$ 10 mm array of crescent-shaped microstructure grooves in the central region. The fabricated mold is shown in Fig. 1(d); the X_0 is 90.43 μm, the Y_0 is 60.46 μm, the L is 44.96 μm, and the P is 44.96 μm.

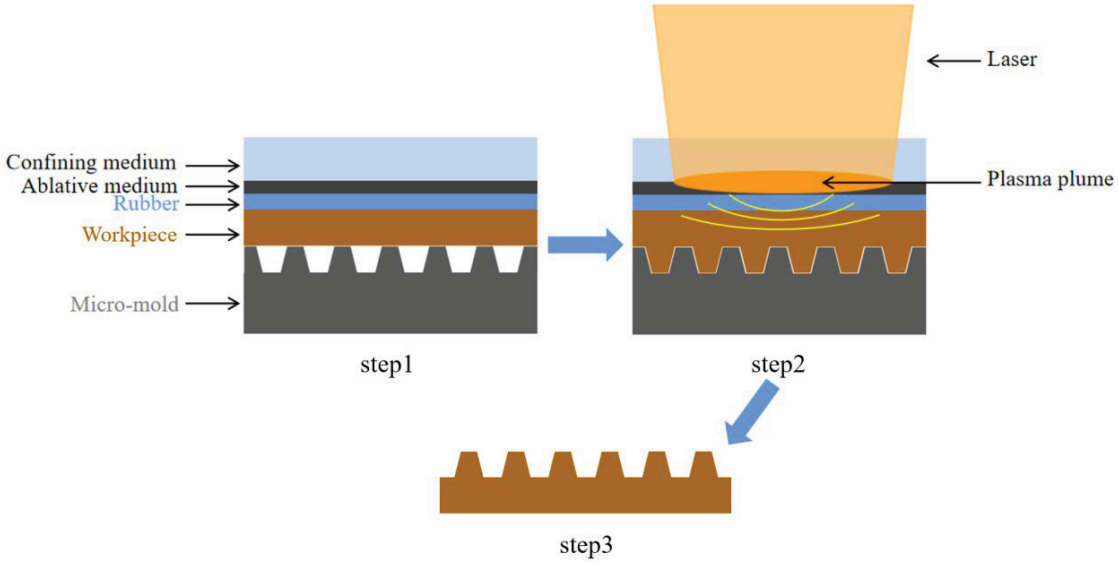


Fig. 2. Principle diagram of LSI

Table 2. Materials for LSI

Functionality	Constraint layer	Ablative layer	Soft film	Workpiece
Material	PMMA	Aluminum foil	Polyurethane	Copper foil
Thickness	3 mm	20 μm	100 μm	10 μm

2.2. Principle and processing method of LSI

LSI uses a high-power, short-pulse laser to interact with a substance to generate a strong shock wave in a short period of time, and then the shock wave energy is used to shape the workpiece. The principle of LSI is shown in Fig. 2, where the focused high-energy density laser passes through the transparent confining layer and radiates on the surface of the ablative layer. The surface of the ablative layer material will absorb the laser energy and rapidly vaporize and ionize, forming a high-pressure plasma and simultaneously generating a strong shock wave, which is homogenized when passing to the bottom of the soft film and then acts on the metal sheet. When the pressure is much higher than the dynamic yield strength of the workpiece, the metal sheet instantly generates a high strain rate of plastic deformation and fits closely with the surface of the micromold, which can replicate the micro- and nanostructure of the mold surface [27]. From top to bottom, the LSI experimental platform consists of a constrained layer, an ablative layer, a flexible film, a workpiece, and a micromold. The materials selected are shown in Table 2. The constraint layer is utilized to increase the shock wave pressure and extend the duration of action. As the constraint layer, a polymethyl methacrylate (PMMA) plate with a thickness of 3 mm is used to guarantee light transmission. Aluminum foil with a thickness of 20 μm is used as the ablative layer to absorb the laser energy and protect the surface of the workpiece from thermal ablation effects. A soft polyurethane rubber film is chosen as the shock wave energy transmission medium so that the Gaussian-distributed laser shock wave energy is loaded more uniformly on the workpiece surface. A copper foil with a thickness of 10 μm was chosen as the workpiece. As the imprinting mold (the mold parameters are shown in Table 1), a crescent-shaped microstructure array was fabricated on the glass surface by etching. By regulating the processing parameters of LSI (as shown in

Table 3. Process parameters for LSI

LSE[1] (mJ)	Number of laser shocks (times)		
835	1	2	3
1020	1	2	3
1200	1	2	3

[1]LSE is an abbreviation for Laser Shock Energy.

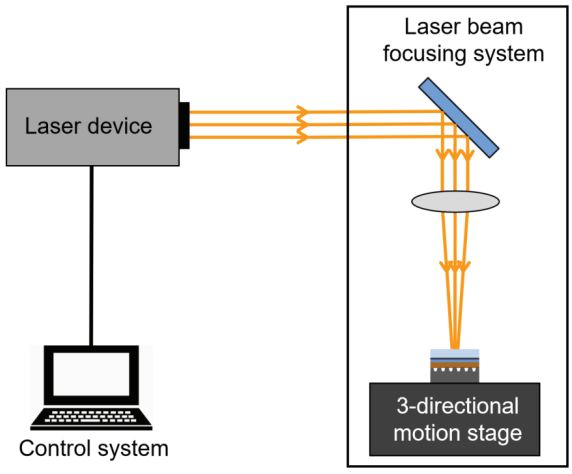


Fig. 3. LSI experimental system

Table 3), large-area crescent-shaped microstructure arrays were fabricated on the surface of copper foil workpieces. The laser in use was a Spitlight 2000 Nd:YAG nanosecond-pulsed laser from InnoLAS, Germany. As depicted in Fig. 3, the entire LSI system consists of a laser, a beam-focusing system, and a three-directional motion stage that facilitates movement in the X, Y, and Z directions. The laser beam is emitted from the laser emitter port, passes through the reflector and focusing mirror, and acts vertically on the workpiece surface.

2.3. Methods of characterization

A super-depth-of-field 3D microscope (VHX-1000C, KEYENCE, Japan) was used for the measurement of 2D and 3D morphological characteristics of microstructures on the mold and workpiece surfaces. The video-based optical contact angle meter (OCAH200, Dataphysics, Germany) was used for the measurement of contact angle on the workpiece surfaces to detect the wettability of the workpiece surfaces. The morphology of the crescent-shaped microstructures fabricated by LSI was observed using a scanning electron microscope (SEM) (Hitachi, S-3400N, Japan).

3. Results and discussions

3.1. Surface morphology of crescent-shaped microstructures

The main parameters of the crescent-shaped microstructure used in the LSI process are as follows: X0 = 90 μm, Y0 = 60 μm, P = 0 μm and 45 μm. The LSI process parameters were 1020 mJ laser energy, a spot diameter of about 2 mm, 3 shock times, and a 0% lap rate. Figure 4 shows the surface of the workpiece after LSI. Figures 4(a) and (b) depict the surface of the imprinted workpiece with 0 μm and 45 μm offset distances, respectively. The imprinted workpiece surfaces with two different offset distances were neatly distributed in forming areas, and the crescent-shaped microstructure array in the imprinted area was formed without any breaks or incomplete or missing imprinting. As depicted in Figures 4(c) and (d), the individual spot imprint ranges of the two surfaces were measured with diameters of 2012.16 μm and 2021.38 μm, respectively, as expected. The morphology of the crescent-shaped microstructure is depicted in Figure 5. From Figures 5(a), (b), (d), (e), and (f), it is apparent that the edges of the individual crescent structure were fully formed with well-defined contour boundaries and complete surface replication after imprinting, and the dimensions of the individual crescent were measured as shown in Fig. 5(c), with R1 of approximately 30 μm and R2 of approximately 36 μm. Figures 6(a) and (b) illustrate the three-dimensional morphologies of the imprinted surfaces with two offset distances of 0 μm and 45 μm, respectively. When the same LSI-processing parameters were used, the crescent-shaped microstructures on the surface of the workpiece imprinted at the two offset distances were arranged neatly and regularly. The shape of the single microstructure resembles a crescent-shaped boss with a large bottom and a small top, and the height H was approximately 9.2 μm, which was

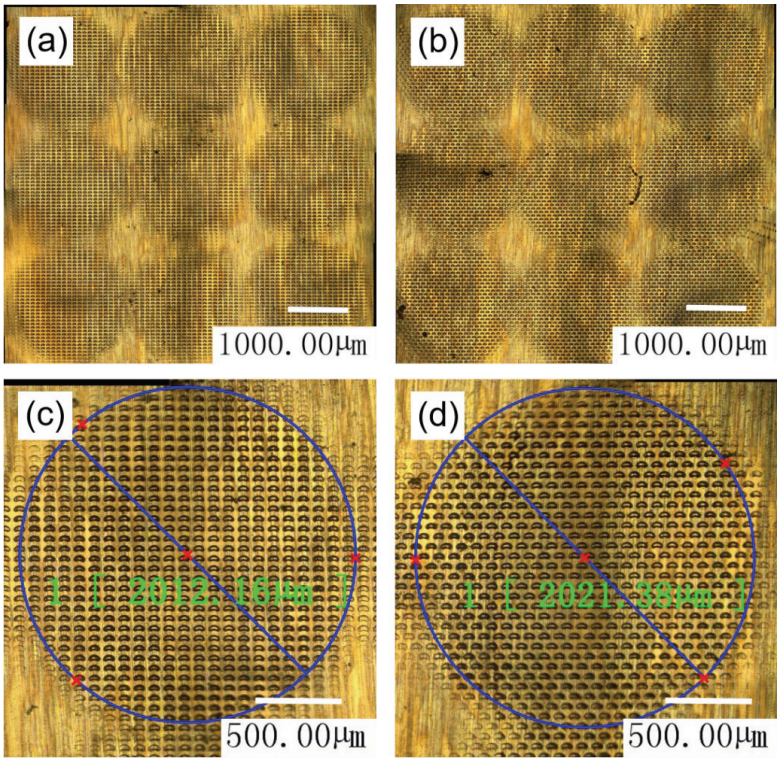


Fig. 4. Two-dimensional morphologies of the microstructures for two different offset distances (P): (a) P = 0 μm; (b) P = 45 μm; (c) P = 0 μm, measurement results of a single spot imprint diameter; (d) P = 45 μm, measurement results of a single spot imprint diameter

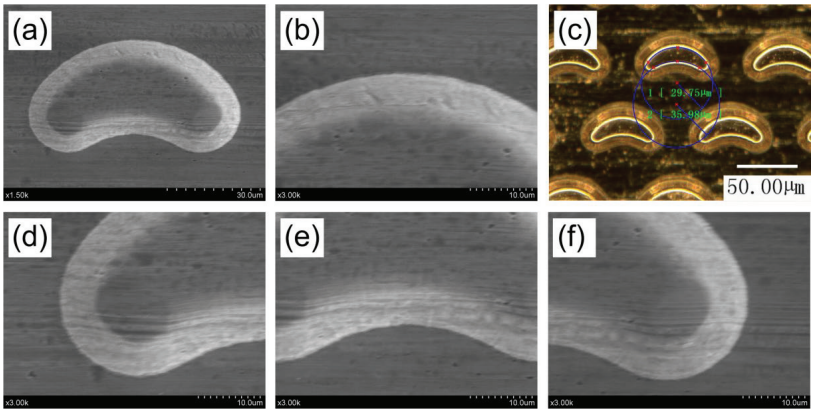


Fig. 5. Surface crescent-shaped microstructure of the workpiece: (a) SEM morphology of a single crescent-shaped microstructure; (b) magnification of the crescent-shaped outer arc forming region; (c) the size measurement of a single crescent-shaped microstructure; (d) magnification of the crescent-shaped left corner forming region; (e) magnification of the crescent-shaped inner arc forming region; (f) magnification of the crescent-shaped right corner forming region

conducive to the demolding of the workpiece after imprinting.

Three LSE (835 mJ, 1020 mJ, and 1200 mJ) and three laser shock numbers (1, 2, and 3 times) were used to fabricate the microstructure surfaces (The processing parameters of LSI are shown in Table 3). The three-dimensional morphologies of the workpiece surfaces fabricated by different

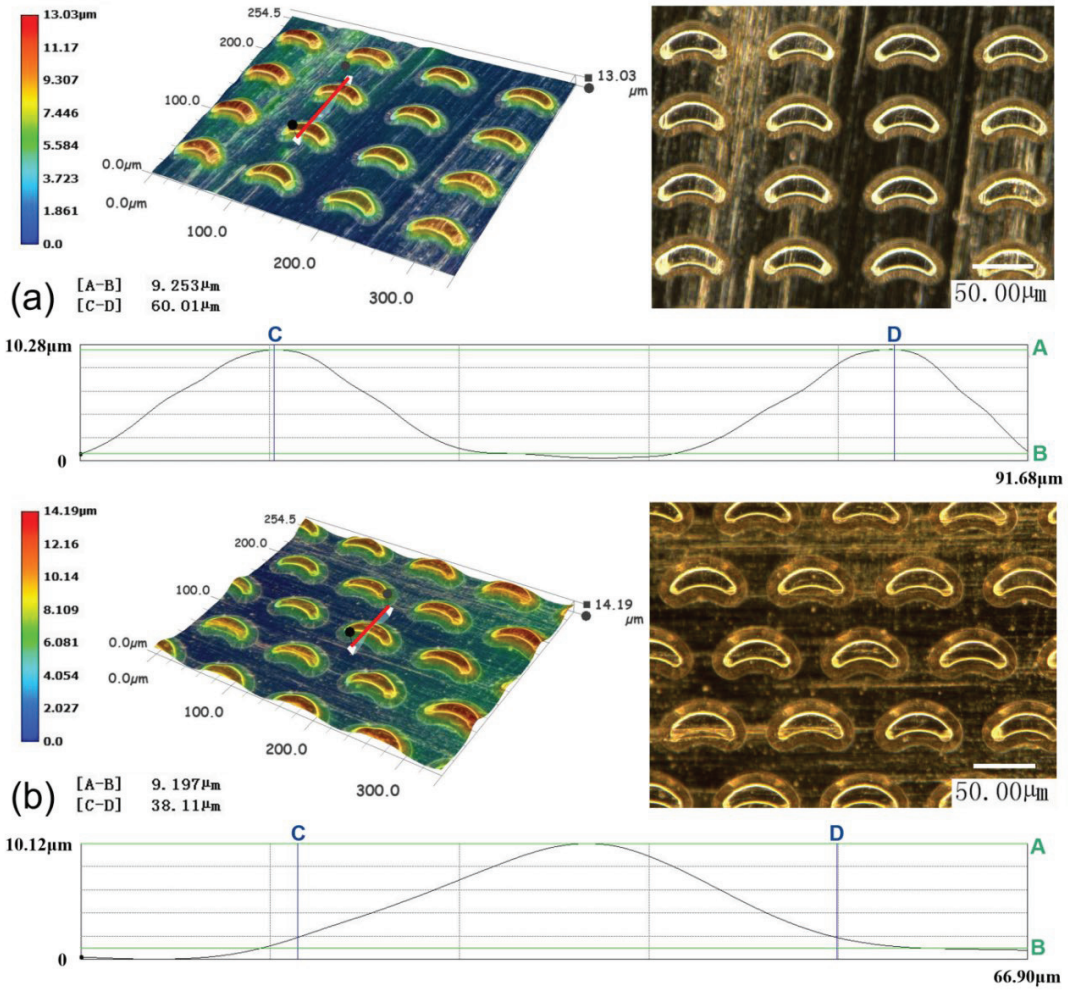


Fig. 6. Three-dimensional morphologies of the workpiece surface for two different offset distances (P). (a) P = 0 μm; (b) P = 45 μm

LSI parameters are shown in Figure 7. From Figures 7(a), (b), and (c), it can be seen that, with the increase in LSE, the crescent-shaped microstructure morphology of the workpiece surface is increasingly close to the morphology of the mold surface; the top of the crescent shape is increasingly close to the bottom of the mold. When the LSE reaches 1020 mJ, the top of the replication degree basically reaches the optimum. When the LSE increases to 1200 mJ, the overall morphology does not change much. Comparison of Figs. 7(d), (e), and (f) shows that when the LSE is constant at 1020 mJ, the degree of plastic deformation of the workpiece increases with the increase of the number of shocks, and the degree of replication of the crescent-shaped microstructure on the workpiece surface increases, and the forming performance reaches its best when three shocks are applied.

Figure 8 shows the forming height of the surface microstructure with different LSI processing parameters. The height of the formed surface microstructure increases with increasing shock numbers at a constant LSE. For the same number of shocks, there is a positive relationship between the forming height and the LSE. As a result of the microstructure groove depth of the mold, the maximal forming height (approximately 9.1 μm) was reached when the LSE increased to 1020 mJ for three shocks. Further analysis reveals that the microstructure height change generated by the first

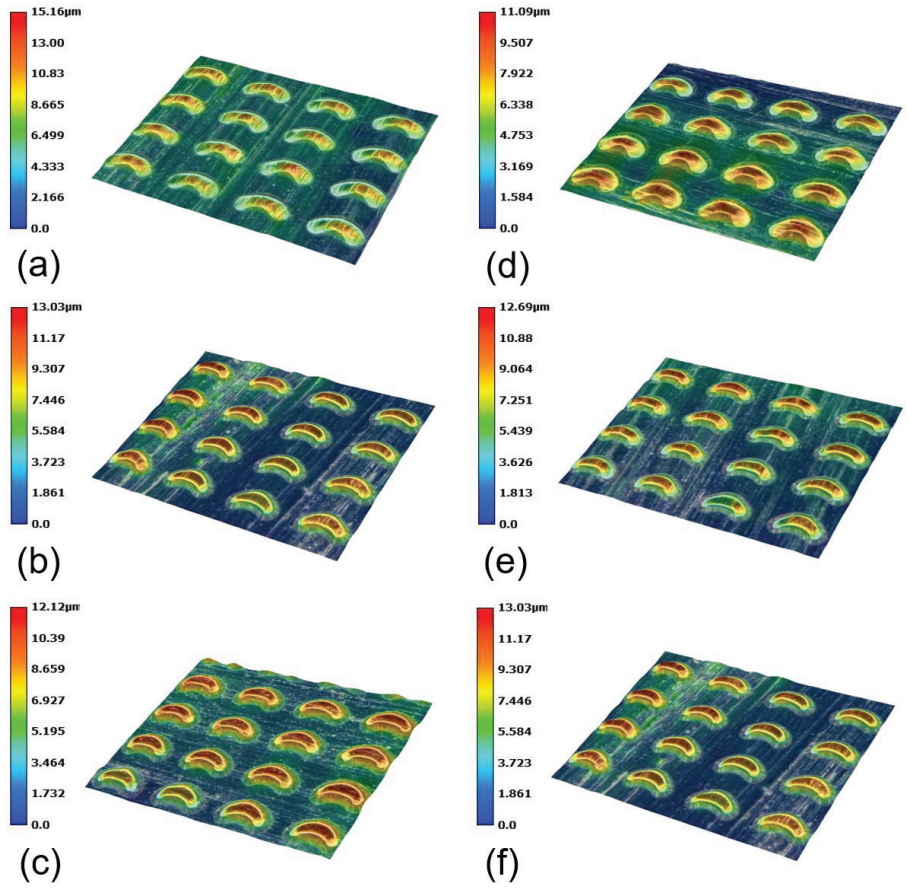


Fig. 7. Three-dimensional morphologies of the workpiece surface fabricated by different LSI parameters: (a) LSE 835 mJ, 3 shocks; (b) LSE 1020 mJ, impact 3 shocks; (c) LSE 1200 mJ, 3 shocks; (d) LSE 1020 mJ, 1 shock; (e) LSE 1020 mJ, 2 shocks; (f) LSE 1020 mJ, 3 shocks

shock will be significantly higher than the subsequent height change. For example, when the LSE is 1020 mJ, the initial shock generates a height change of 6.03 μm, and the second shock generates a change of only 1.63 μm. This is mainly caused by the technological characteristics of LSI. Only after the plasma shock wave generated by the ablative layer is transmitted to the surface of the soft film can it further act on the surface of the workpiece. As shown in Figure 9(a), before the first LSI, the workpiece had not been plastic deformed and had a high degree of contact with the surface of the soft film, so the efficiency of shock wave transfer was high and the resulting plastic deformation was large. As shown in Figure 9(b), before the second LSI, due to the plastic deformation of the workpiece, an air cavity is generated between the workpiece and the soft film, and the mutual contact degree is significantly reduced, so the efficiency of shock wave transmission is also significantly reduced; therefore, the height change of the second LSI is significantly reduced compared with the first LSI. It can be considered that the greater the degree of initial plastic deformation of the workpiece, the more obvious the phenomenon.

The heights of different positions of a single crescent-shaped microstructure fabricated by three shocks with 1020 mJ energy can be observed in Figure 10. The location of the center of symmetry is shown in Figure 10(a), and its contour line is shown in Figure 10(d) with a height of about 9.77 μm. Figure 10(b) shows the position near the right rounded corner, and its contour line is shown in Figure 10(e) with a height of about 8.79 μm.

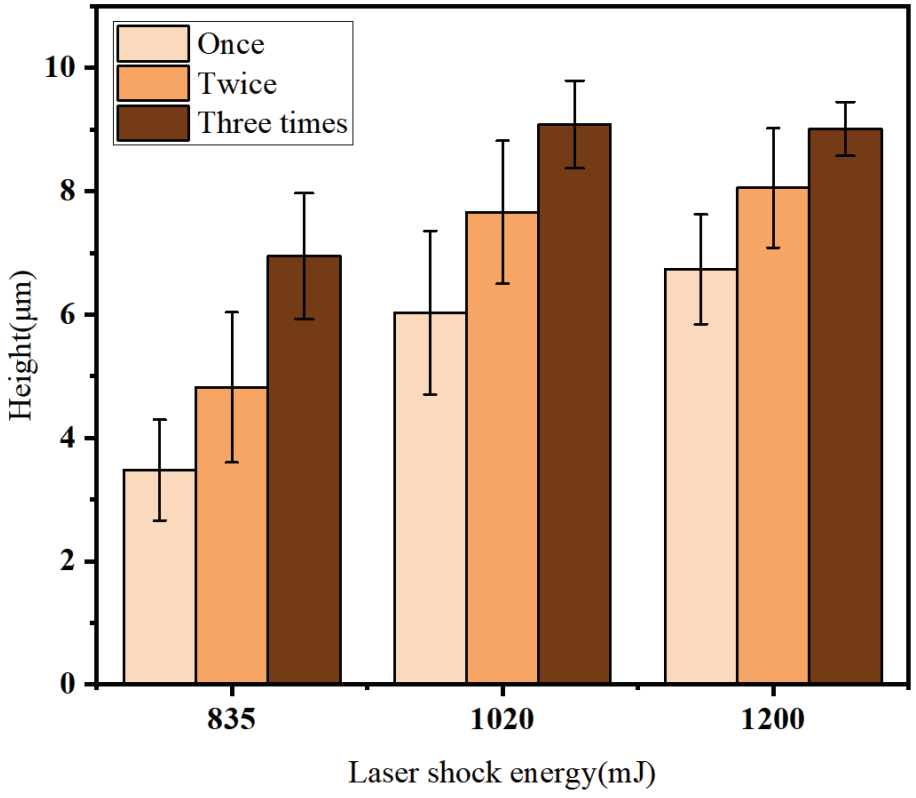


Fig. 8. Influence of LSI processing parameters on the forming height of crescent-shaped microstructures on the workpiece surface

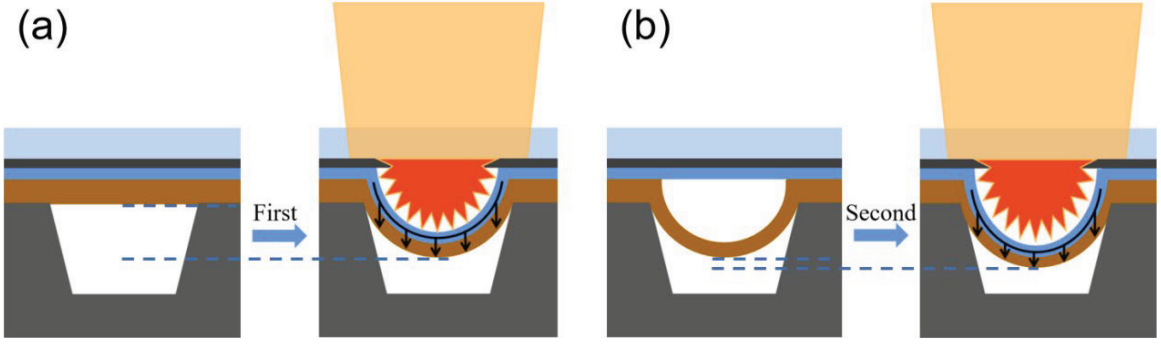


Fig. 9. Schematic diagram of dynamic changes of the workpiece and soft film imprinted by multiple LSIs. (a) the first LSI; (b) the second LSI

The location of the localized internal section of the structure is shown in Figure 10(c), with the contour line shown in Figure 10(f). which means that the height of the position at the center is higher than the height of the position near the right round corner. Analysis speculates that there are two reasons for this. On the one hand, the cavity size of the mold in the center position is wider than that of the position near the right corner of the lead. The principle of the schematic diagram is shown in Figure 11. The workpiece is extruded into the groove of the mold through shock energy. Under the same LSI-processing parameters, due to the influence of the size effect of the material itself, the wider the cavity size, the easier the workpiece flows into the cavity, and the better the

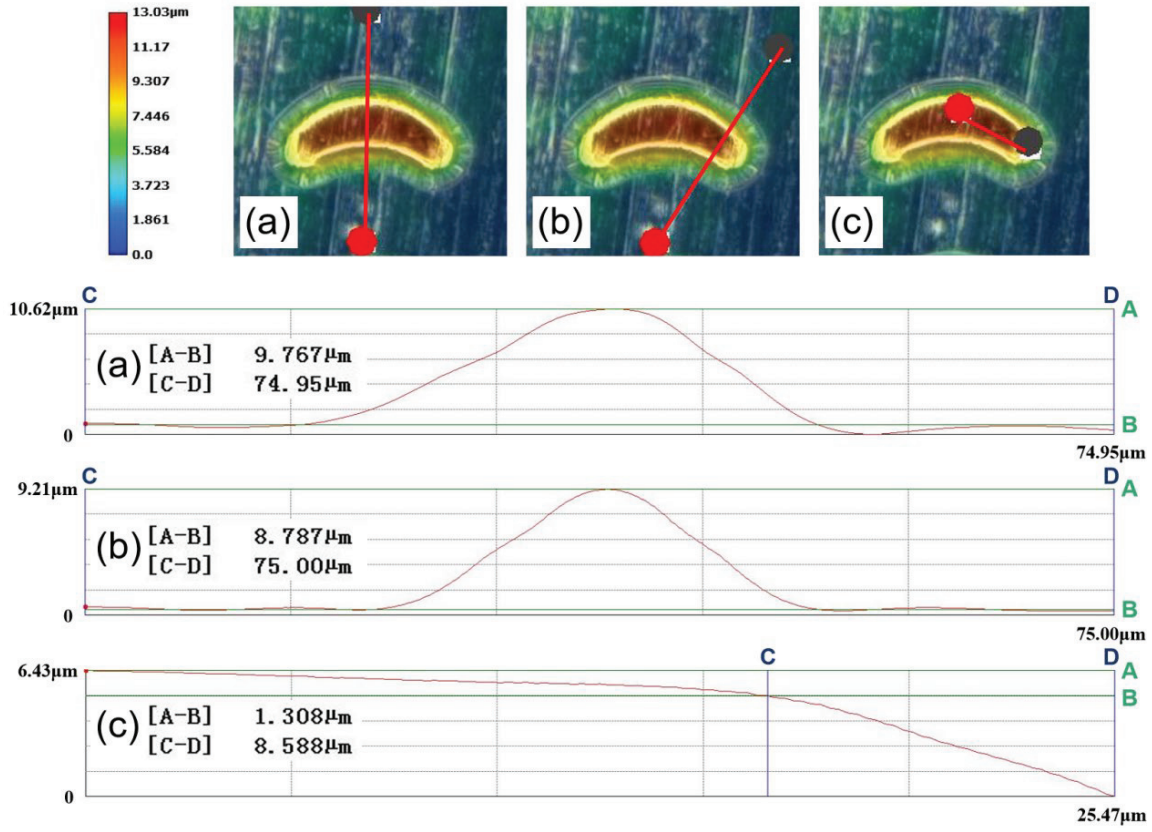


Fig. 10. Heights of crescent-shaped microstructures at different positions: (a) center of symmetry; (b) near the right rounded corner; (c) localized inner cross section; (d) contour line at position (a); (e) contour line at position (b); (f) contour line at position (c)

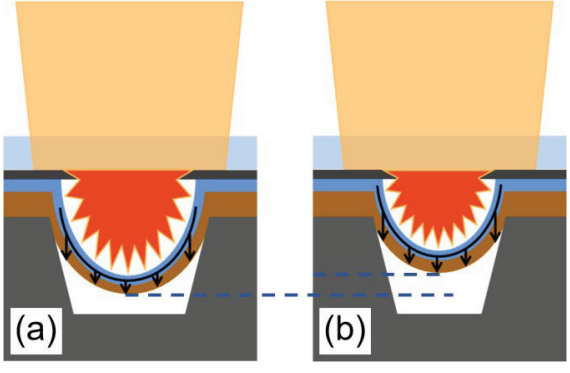


Fig. 11. Schematic diagram of the effect of different width molds on forming depth: (a) wide mold; (b) narrow mold

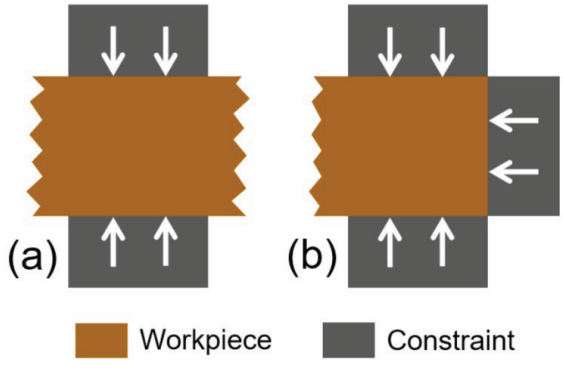


Fig. 12. Two different constraint cases: (a) two directions; (b) three directions

reproduction effect on the mold. Another aspect is a result of the fact that the workpiece at the center of the symmetry position is formed with constraints mainly in two directions, whereas the workpiece near the right round corner position is constrained in approximately three directions. As shown in the schematic diagram of Figure 12, multidirection constraints will cause more limitations on material flow.

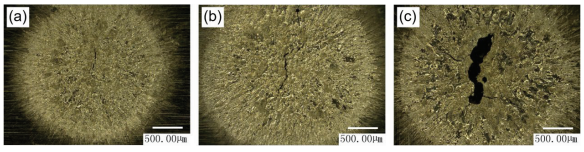


Fig. 13. Comparison of ablated layers processed with diverse LSI parameters: (a) LSE 835 mJ, 3 shocks; (b) LSE 1020 mJ, 3 shocks; (c) LSE 1200 mJ, 3 shocks

As LSE and the number of shocks increase, they will exceed the bearing limit of the ablation layer. As shown in Figure 13(a), when the LSE was 835 mJ and the number of shocks was three, the ablated layer had no holes. As depicted in Figure 13(c), when the LSE was 1200 mJ and the number of shocks was three, the ablated layer had obvious holes. It was indicated that part of the laser energy was not fully absorbed by the ablated layer, and the laser energy utilization was decreased. As shown in Figure 13(b), with a LSE of 1020 mJ and 3 shocks, the ablated layer exhibited only a few cracks. It was indicated that the ablated layer absorbed laser energy more efficiently to guarantee the surface-forming quality of the workpiece. With a LSE of 1020 mJ and 3 shocks, the workpiece surface crescent-shaped microstructure morphology replication degree basically reached the best replication. Therefore, the optimal LSI parameter for the subsequent wettability study was three times the shock of 1020 mJ energy.

3.2. Analysis of the anisotropic wettability

Figure 14 shows the measurement results of the contact angle on the surface of the workpiece fabricated by LSE of 1020 mJ and 3 shocks. The contact angle in the raw material region was 75°, while the contact angle in the crescent-shaped microstructure region was 96.5°. The crescent-shaped microstructure considerably enhanced the hydrophobicity of the copper foil's surface. Figure 15 depicts the measurement results of the contact angle on the surface of the workpiece fabricated with various LSI processing parameters, while Figure 15(a) depicts the effect of the number of shocks on the contact angle at LSE of 1020 mJ. As the number of shocks increases, the contact

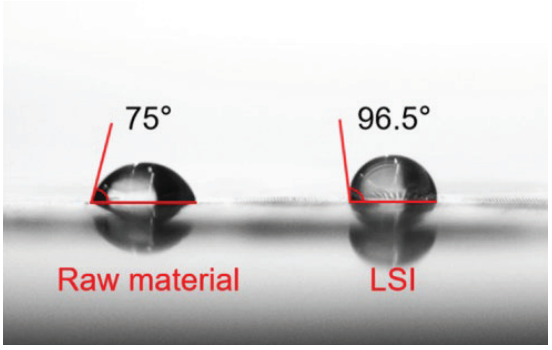


Fig. 14. Contact angle diagram on the surface of the workpiece. Contact angle on the surface of raw material (left), contact angle on the surface of crescent-shaped microstructure (right)

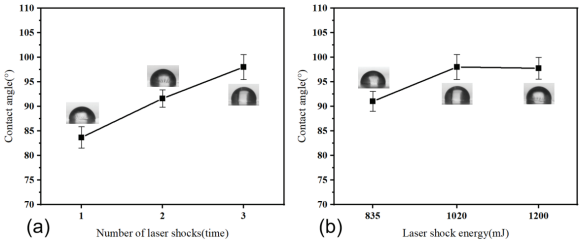


Fig. 15. Effect of different LSI processing parameters on the contact angle: (a) effect of the number of laser shocks on the contact angle; (b) effect of LSE on the contact angle

angle of the surface of the workpiece progressively increases. Figure 15(b) depicts the contact angle on the surface of the workpiece at LSE values of 835 mJ, 1020 mJ, and 1200 mJ, when the number of shocks is three. The figure demonstrates that as LSE increases, the contact angle increases, with the contact angle hardly changing once the energy exceeds 1020 mJ. As shown in Figures 8 and 15, it was discovered that the change law of the contact angle of the imprinted surface coincides with the change law of the height of the crescent-shaped microstructure.

Due to the asymmetry of the crescent structure shape and feature array in each direction, the fabricated workpiece surface wettability appears anisotropic. Observed from a parallel direction, the contact angle on both sides of the workpiece surface was nearly identical, as a result of the symmetry of the crescent structure shape and feature

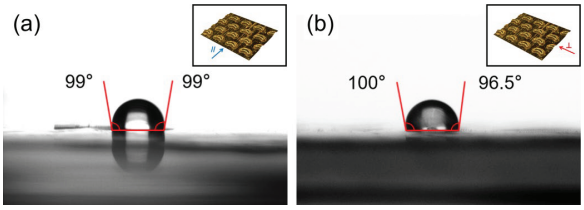


Fig. 16. Contact angle diagram of water droplets on the workpiece surface in two directions: (a) parallel (//) direction; (b) perpendicular (⊥) direction

array in a parallel direction. When observed from the vertical direction, however, the contact angle of the outer arc direction of the crescent-shaped microstructure was always slightly smaller than that in the inner arc direction (i.e., the contact angle on the right side was smaller than the contact angle on the left side), as a result of the asymmetry of the crescent structure shape and feature array in the vertical direction. Figure 16 depicts the morphologies of water droplets in different directions on the surface of two crescent-shaped microstructure workpieces fabricated with an LSE of 1020 mJ, 3 shocks, and an offset distance of 45 μm. As depicted in Figure 16(a), the contact angles of water droplets observed from a parallel direction were identical: 99° on both sides. As depicted in Figure 16(b), the contact angles of the water droplets observed from the perpendicular direction were as follows: The contact angle on the left side was 100° and on the right side was 96.5°, and the difference between the contact angles on both sides was 3.5°. This indicates that the fabricated crescent-shaped microstructure workpiece has a surface with an obvious anisotropy.

While the shape of the crescent-shaped microstructure remained unchanged, the influence of the offset distance (P) of the microstructure feature arrangement on the anisotropy of the surface was investigated and further analyzed. The molds with offset distances of 0 μm, 30 μm, and 45 μm were selected, and three kinds of crescent-shaped microstructured workpiece surfaces were fabricated using LSI with the process parameters of LSE of 1020 mJ and the number of shocks of three times. The effect of different offset distances in the vertical direction on the contact angle

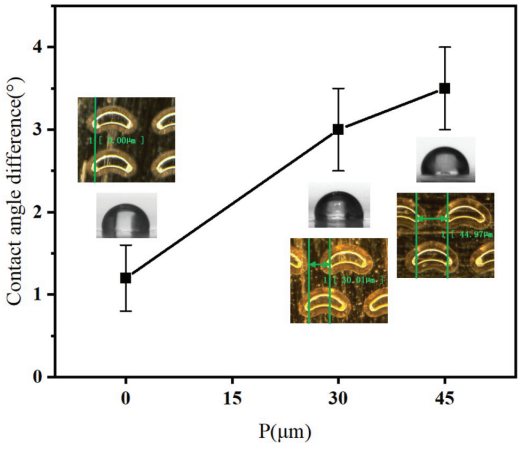


Fig. 17. Influence of the offset distance (P) of the alignment of crescent-shaped microstructure features on the contact angle difference of water droplets on their surfaces

difference between water droplets on both sides of the crescent-shaped microstructured workpiece surface is depicted in Figure 17. It can be seen from the figure that when the offset distance is 0 μm, the contact angle difference is relatively small and the anisotropy is at its weakest, and the contact angle difference at this time is mainly due to the asymmetry of the crescent-shaped microstructure shape. As the offset distance increases, the contact angle difference also increases, and when the offset distance reaches 45 μm, the contact angle difference between the two sides of the water droplet is at a maximum, approximately 3.5°. Since the design parameter of the vertical alignment spacing of the microstructure features is 90 μm, the superposition of crescent-shaped microstructure shape and microstructure feature alignment asymmetry has the greatest influence, resulting in the best anisotropy on the workpiece surface.

3.2.1. Morphological analysis of droplet solid–liquid contact lines

The structural asymmetry and arrangement of the crescent-shaped microstructures on the surface of the workpiece lead to the generation of asymmetric droplet-spreading resistance, resulting in a change in the shape of solid–liquid contact lines on the fabricated surface of the workpiece that

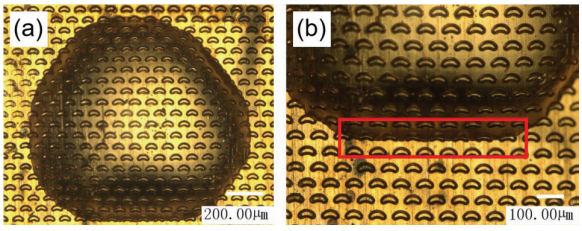


Fig. 18. Residual droplet morphology on crescent-shaped, microstructured workpiece surface: (a) Droplet overall solid-liquid contact line; (b) solid-liquid contact line of droplet on the surface of workpiece on the bottom of the arc

is different from that of the circular solid–liquid contact lines on the anisotropic surface, and a solid–liquid contact line resembling a straight line is generated. The suspended droplet on the syringe was slowly put in contact with the microstructure surface and deposited (water, volume of about 1 μL), and the morphology of the droplet was observed. The whole residual droplet was photographed as shown in Figure 18(a), where the solid–liquid contact lines on the left and right sides of the droplet were similar to arcs, and the solid–liquid contact line at the bottom of the droplet (the droplet side in the direction of the bottom of the arcs) was an overall straight-line-like shape. The enlarged image is shown in Figure 18(b). The analysis speculates that it may be due to the fact that the barriers against which the droplets spread towards the bottom of the arc are larger compared to the other directions, thus the droplets are more difficult to cross as compared to the other directions, which is reflected in the fact that the solid–iquid contact line is restricted to an overall similarly straight shape.

During droplet motion, the direction of liquid movement depends on the asymmetric resistance generated by the special microstructure [28]. According to Jing et al. [29], the cause of anisotropic wettability can be analyzed by establishing the equation of resistance to droplet motion on a plane. Therefore, a single crescent-shaped microstructure is taken as the object of study and the following equation is established:

$$\alpha = \arcsin\left(\frac{l}{2R}\right) \tag{1}$$

$$L_a = \frac{2\alpha\pi R}{180} \tag{2}$$

$$f = \gamma(\cos\theta - \cos\theta_1) \tag{3}$$

$$F = f \cdot L_a \tag{4}$$

$$F_{\mathrm{t}} = f \cdot L_{a2} = f \cdot \frac{2\alpha_2\pi R_2}{180} \tag{5}$$

$$F_{\mathrm{b}} = f \cdot L_{a1} = f \cdot \frac{2\alpha_1\pi R_1}{180} \tag{6}$$

As shown in Figure 19(a), the solid–liquid contact line of a single crescent-shaped microstructure on the surface of the workpiece is extracted, and the solid–liquid contact line generated when the droplet spreads in the direction of the bottom of the arc is the outer arc L_{a1}, and the solid–liquid contact line generated when the droplet spreads in the direction of the top of the arc is the inner arc L_{a2}. Figure 19(b) shows the mathematical model of the solid–liquid contact line for the part of the crescent-shaped microstructure. Measurement of the fabricated crescent-shaped microstructure yields an outer arc radius R_1 of about 30 μm and an inner arc radius R_2 of about 36 μm, which are calculated by substituting into Equations (1) and (2) to yield an outer arc with a longer solid–liquid contact line. According to Equations (3) and (4), the motion resistance F is related to the solid–liquid contact line L_a as well as the motion resistance per meter of the droplet f. From Equations (5) and (6), the resistance to spreading towards the bottom of the arc, F_b, is greater than the resistance to spreading in the direction towards the top of

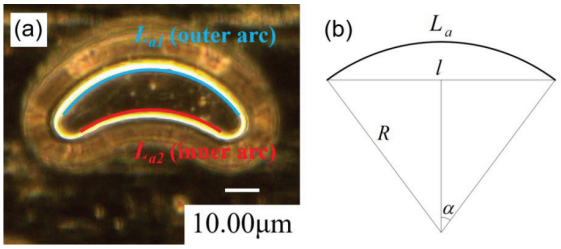


Fig. 19. Modeling of solid–liquid contact lines of crescent-shaped microstructures: (a) location of some solid–liquid contact lines of crescent-shaped microstructures; (b) mathematical modeling of solid–liquid contact lines of crescent-shaped microstructures

the arc, F_t. Therefore, the anisotropic wettability in the direction of the top and bottom of the arc are formed, which causes the solid–liquid contact line to take on a special shape.

3.3. Design of directional spreading surfaces

According to the study above, the increase in the surface contact angle is positively correlated with the increase in the height of the crescent-shaped microstructure. Therefore, different LSI-processing parameters can be used to fabricate surfaces with different wettability, and a crescent-shaped microstructure gradient surface is designed for the directional spreading of droplets on gradient wetting surfaces [30]; i.e., water droplets will move and spread to the side with high wettability because of the surface energy gradient. Since the anisotropy of the crescent-shaped microstructure causes anisotropic wetting of the workpiece surface, the array feature arrangement with the greatest anisotropy (Mold 3 in Table 1) is used as the mold for the fabrication of the microstructured surface. Surfaces with a wettability gradient are fabricated by controlling the LSI-processing parameters so that there is a significant difference in the wettability of the two zones. Figure 20 depicts the designed wettability gradient surface schematically. The left side (Fig. 20a) is a low wettability surface, while the right side (Fig. 20b) is a high wettability surface. Both sides constitute

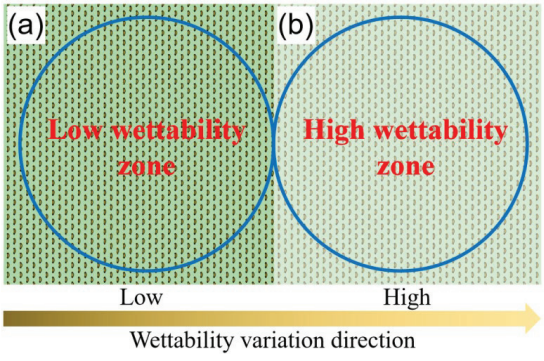


Fig. 20. Schematic diagram of the wettability gradient surface of the crescent-shaped microstructure: (a) low wettability zone; (b) high wettability zone

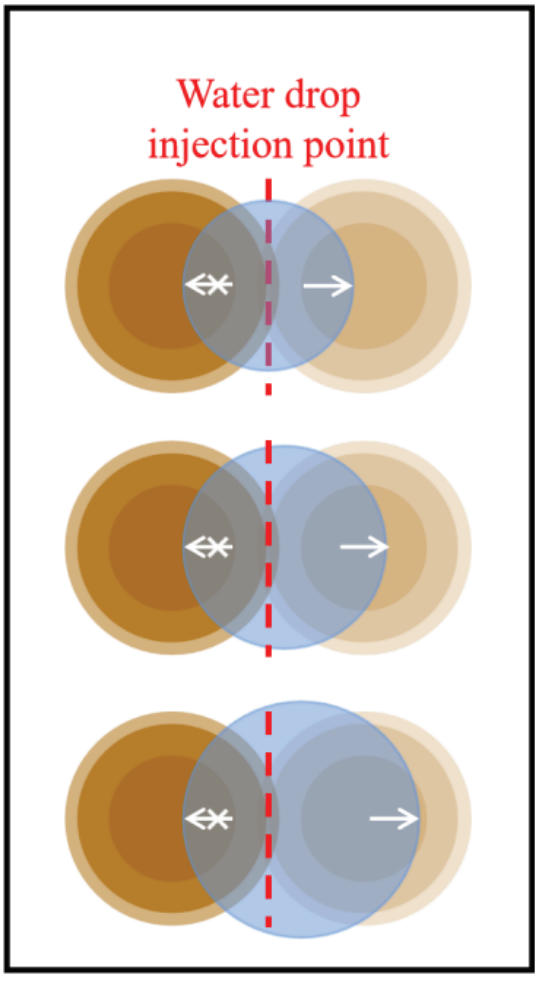


Fig. 21. Schematic diagram of the theory of directional spreading of liquid droplet

a wettability gradient, and the direction of the top of the crescent is also the direction of increasing wettability. The blue circle is the theoretical forming area of the crescent-shaped microstructured surface.

Water droplets are injected at the junction of two zones processed with different LSI-processing parameters, with the left side having low wettability and the right side having high wettability. The theoretical spreading schematic for a liquid is shown in Figure 21, where the red dashed line indicates the location of water droplet injection, the dark brown circle on the left side represents the low wettability area, and the light brown circle on the right side represents the high wettability area. The spreading of droplets in the low wettability zone

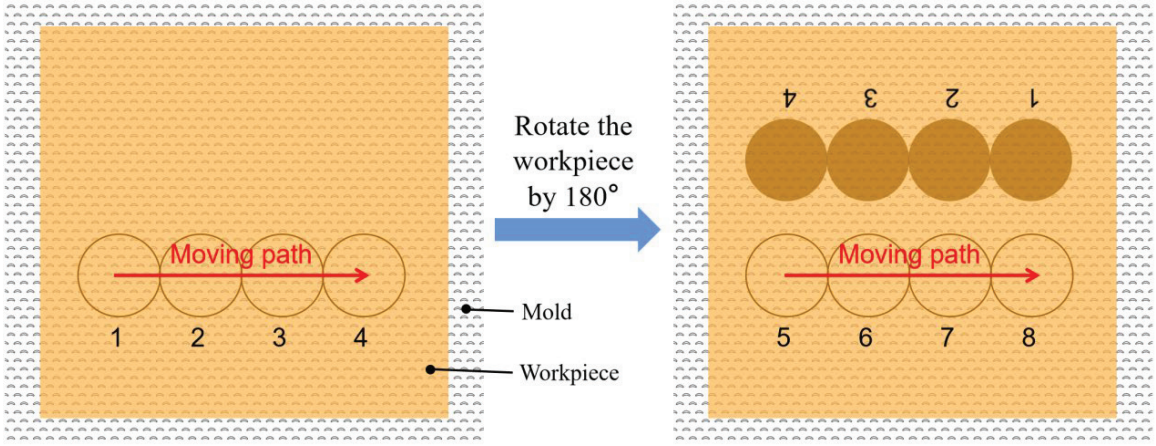


Fig. 22. Schematic diagram of the method of fabricating type-I flow channel by LSI

on the left will be limited, causing the droplets to move as a whole toward the high wettability zone on the right.

3.4. Fabrication of a type-I flow channel

Based on the fact that the crescent-shaped microstructured surface is anisotropic, the droplet boundary on the bottom side of the arc generates a clear solid–liquid contact line that is similar overall to a straight line. Flow channels can be designed and fabricated by changing the distribution of crescent-shaped microstructure areas to limit the continuous spreading of liquid droplets to both sides. In Figure 23(a), a schematic of the distribution of the planar microstructure area of the type-I flow channel is depicted. The black forked arrow indicates the direction to restrict droplet movement; the blue section is the theoretical area in which droplets spread; and the brown circles on both sides represent the microstructure array zone fabricated by LSI. Figure 23(b) shows a partially magnified image of the microstructured zone in 18(a), with the crescent-shaped microstructures arrayed in the direction of the outer arc toward the I-type flow channel. A mold with the most anisotropic array structure parameters (Mold 3 in Table 1) and optimal LSI-processing parameters (LSE of 1020 mJ, 3 shocks) was used to fabricate the type-I flow channels. As shown in Figure 22, the distribution of the crescent-shaped microstructure zone was controlled by changing the position

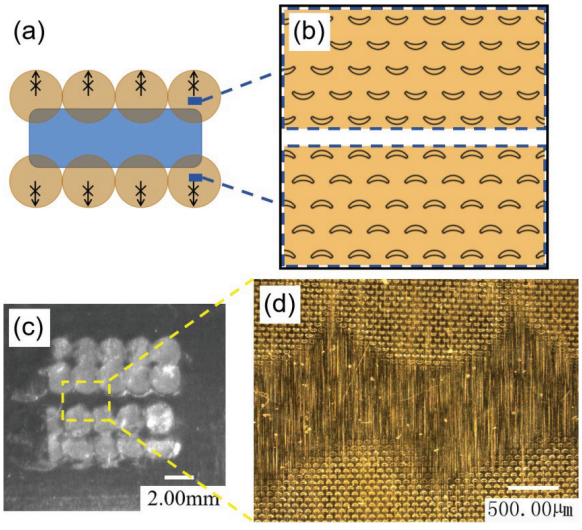


Fig. 23. Type-1 flow channel composed of crescent-shaped microstructure arrays: (a) schematic diagram of the principle of type-I flow channel; (b) a partially magnified image of the microstructured zone; (c) fabricated type-I flow channel morphology; (d) local morphology of type-I flow channel

of the mold and the workpiece; the numbers (1, 2, 3, ...) are the order in which the laser beams are scanned, and the red arrows are the moving path of the laser beam. The fabricated type-I flow channel is depicted in Figure 23(c). The inner and outer layers of the flow channel consist of several microstructure areas, and only the effect of the inner layer microstructure areas on droplet

spreading was investigated in this study. The circular crescent-shaped microstructure-forming area was regularly distributed on both sides of the flow channel, which together formed a type-I structureless zone with a width of approximately 1 mm. The edges of the flow channel area were regular serrated-like, the adjacent serrated tooth spacing was approximately 1.8 mm, and the maximum tooth base spacing on both sides of the flow channel was approximately 2.3 mm. The morphology of the inner part of the type-I flow channel (in Fig. 23c) was observed. As depicted in Figure 23(d), the crescent-shaped microstructure on the inside of the type-I flow channel had the outer arc towards the flow channel side and the inner arc back to the flow channel side. The forming quality of the crescent-shaped microstructure near the inside of the flow channel was poor compared to the outside, and the microstructures at the edges of the flow channel in different spot areas were not connected together. The edges appear to be jaggedly separated, resulting in a jagged shape in the structureless area of the flow channel.

The same liquid (water, volume 18 μL) was dropped into the flow channel and raw material area by the method of slowly dropping it several times in the direction of the flow channel and then causing the droplets to converge. When the droplets converged, the morphology of the liquid in the two areas was observed. As shown in Figure 24(a), as the droplets were continuously dropped, the droplet expansion range in the microstructure area on both sides inside the flow channel area was significantly smaller than that in the raw material area, and the droplets in the raw material area always showed an oval shape due to the influence of the surface tension of the material. The measured long axis was approximately 5.4 mm, and the measured short axis was approximately 4.8 mm, whereas the droplets inside the flow channel area stopped expanding and spreading after expanding to a certain position on both sides of the flow channel, and the phenomenon of liquid droplet being fixed occurred. The final shape is a strip; the length in the flow channel direction was approximately 7 mm, and the length perpendicular to the flow channel direction was approximately 3 mm. Re-drop the droplet in the runner area with the method described above. The liquid–solid contact edge in the microstructure area inside the flow channel was observed as shown in Figure 24(b), and both the upper and lower edges of the droplet inside the flow channel area were affected by the crescent-shaped microstructure, which generated solid–liquid contact lines that approximate straight lines. The fabricated flow channel realized the restriction of liquid droplets spreading on the surface of the workpiece.

The solid–liquid contact lines on both sides of the flow channel were discovered in the crescent-shaped microstructure region outside the central serrated region. As depicted in Figures 25(a) and (b), the blue line represents the boundary of the serrated region, and the red line represents the location where the fixed contact line was generated. The location where the liquid generated the fixed contact line was outside the serrated region. This is due to the volume of the water droplets used in this study and the process characteristics of LSI. The

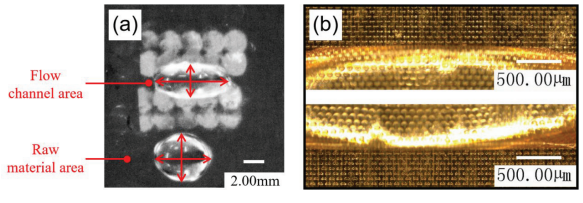


Fig. 24. Water droplet spreading mode on the surface of the type-I flow channel: (a) comparison of water droplet morphology in the flow channel and raw material areas; (b) morphology of water droplets on both sides of the microstructure area inside the flow channel area

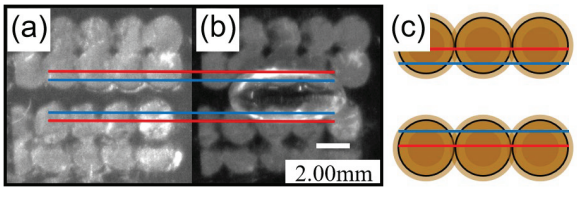


Fig. 25. Diagram of water droplet movement position within the flow channel: (a) flow channel without water droplets; (b) flow channel after water droplet injection; (c) schematic diagram of water droplet spreading position within the flow channel

continuous increase in droplet volume on the surface of the workpiece per unit area also increases the pressure on the crescent-shaped microstructure on both sides of the solid–liquid contact line. When the resistance limit of the crescent-shaped microstructure is exceeded, the original fixed contact line will be broken and spread outward to form a new fixed position. As shown in the schematic diagram in Figure 25(c), since the laser output is a Gaussian beam (which generates a Gaussian distribution of LSE), the shock wave generated in the ablation layer will also exhibit a Gaussian distribution; the shade of color in the brown circular area represents the size of the shock wave energy; the darker the color, the higher the energy. The black circle represents the area with a more effective forming result. Despite the use of a soft rubber film to homogenize the shock energy, there is also an uneven phenomenon of forming pressure (high in the center and low at the edges) after a single-point shock. As a consequence, the microstructure-forming result near the edge of the spot is relatively poor compared to that in the center of the spot (the formed microstructure has a lower height and does not sufficiently conform to the inner surface of the mold), and its wettability and anisotropy are also poor. At the same time, because the laser beam output is a circular spot, the continuous crescent-shaped microstructure is absent in the serrated area on both sides of the formed flow channel, and the region as a whole is less effective in limiting droplet spreading, whereas the middle area of the spot has a good lap, and the well-formed crescent-shaped microstructure has good continuity and is connected together, the effect of a good spreading limitation when the liquid spreads to this area.

4. Conclusions

In this investigation, a kind of crescent-shaped, microstructured concave mold was bionically designed based on the microstructure of the surface of the leaf cage slip zone of *Nepenthes*, and fabricated by the etching method. The crescent-shaped, microstructured surface was fabricated on copper foil by LSI. The forming law and wettability law of the crescent-shaped microstructures on the workpiece surface were investigated. The effect of the offset distance of the crescent-shaped, microstructure arrangement on the anisotropic wettability was investigated. The anisotropic wettability mechanism of crescent-shaped, microstructured surfaces is explained. The influence of various LSI process parameters on the forming morphology and forming height of the crescent-shaped microstructure on the surface of copper foil was studied. It was found that an increase in the LSE and the number of shocks facilitated the formation of crescent-shaped microstructures, as evidenced by a better fit of the morphology to the mold and an increase in height. And the optimal LSI parameters were determined to be 1020 mJ and 3 shocks. On the surface of copper foil, the effects of various LSI parameters on the wettability of the crescent-shaped microstructure were investigated. It was discovered that an increase in LSE and the number of shocks improved the hydrophobicity of the workpiece surface and that the trend of wettability was in accordance with the trend of the crescent-shaped microstructure height change. The anisotropy of its surface is determined to exist due to the asymmetry of the crescent microstructure's shape and feature array in all directions. The effect of the offset distance of the crescent-shaped microstructure feature arrangement on the anisotropy of the workpiece surface was investigated by the optimal LSI-processing parameters. By measuring and calculating the magnitude of the contact angle difference between the two sides of the water droplet, it is found that the contact angle difference at an offset distance of 45 μm is at its maximum, approximately 3.5°, when the asymmetric superposition of the crescent-shaped microstructure and feature arrangement has the greatest influence and has the best anisotropic wettability. And this anisotropy leads to a nearly straight overall solid–liquid contact line at the droplet boundary in the direction of the arc bottom of the crescent-shaped microstructure.

Mathematical and physical modeling explains that the anisotropic wettability is due to the crescent shape, which results in different resistance to droplet spreading in different directions. The anisotropy of crescent-shaped microstructured

surfaces and the liquid gradient wetting law were exploited. A droplet-directional spreading surface was designed in which crescent-shaped microstructure surfaces of different heights are fabricated by different LSI-processing parameters and lapped so that they constitute a wettability gradient. The type-I flow channel was fabricated to achieve the function of limiting the droplet spreading range by altering the distribution position of the crescent-shaped microstructure array on the workpiece surface. The droplet volume per unit area and the effect of the LSI process on the droplet spreading within the flow channel were also analyzed. The droplet volume within the unit area exceeding a certain size causes the position of the fixed solid–liquid contact line to move outward and form a new fixed position, and the process characteristics of LSI cause the fixed solid–liquid contact line to appear in the middle region of the single spot-forming area.

Declaration of Competing Interest

The authors declare that they have no known competing financial interests or personal relationships that could have appeared to influence the work reported in this paper.

References

[1] Wang Q, Xu SS, Xing XT, Wang N. Progress in fabrication and applications of micro/nanostructured superhydrophobic surfaces. *Surf Innov*. 2022;10:89–110.

[2] Yang Y, Li XL, Zheng X, Chen ZY, Zhou QF, Chen Y. 3D-printed biomimetic super-hydrophobic structure for microdroplet manipulation and oil/water separation. *Adv Mater.* 2018;30.

[3] Zhang SN, Huang JY, Chen Z, Lai YK. Bioinspired special wettability surfaces: from fundamental research to water harvesting applications. *Small*. 2017;13.

[4] Zhu H, Guo ZG, Liu MM. Biomimetic water-collecting materials inspired by nature. *Chem Commun.* 2016;52:3863–79.

[5] Zheng YM, Gao SF, Jiang L. Directional adhesion of superhydrophobic butterfly wings. *J Soft Matter.* 2007;3:178–82.

[6] Yang L, Shen XD, Yang Q, Liu JQ, Wu WJ, Li DY, et al. Fabrication of biomimetic anisotropic superhydrophobic surface with rice leaf-like structures by femtosecond laser. *Opt Mater.* 2021;112.

[7] Chen HW, Zhang PF, Zhang LW, Iu HLL, Jiang X, Zhang DY, et al. Continuous directional water transport on the peristome surface of *Nepenthes alata*. *Nature*. 2016;532:85–+.

[8] Feng SL, Zhu PA, Zheng HX, Zhan HY, Chen C, Li JQ, et al. Three-dimensional capillary ratchet-induced liquid directional steering, *Science*. 2021;373:1344–+.x

[9] Hu BB, Duan ZF, Xu BJ, Zhang KJ, Tang ZX, Lu C, et al. Ultrafast self-propelled directional liquid transport on the pyramid-structured fibers with concave curved surfaces. *J Am Chem Soc*. 2020;142:6111–6.

[10] Li, Li JQ, Dong. Bioinspired topological surface for directional oil lubrication. *ACS Appl Mater Interfaces*. 2020;12:5113–9.

[11] Zheng YM, Bai H, Huang ZB, Tian XL, Nie FQ, Zhao Y, et al. Directional water collection on wetted spider silk. *Nature*. 2010;463:640–3.

[12] Wang LX, Zhang SY, Li SS, Yang SX, Dong SY. Inner surface of *Nepenthes* slippery zone: ratchet effect of lunate cells causes anisotropic superhydrophobicity. *R Soc Open Sci*. 2020;7.

[13] Zhang PF, Chen HW, Li L, Liu HL, Liu G, Zhang LW, et al. Bioinspired smart peristome Ssurface for temperature-controlled unidirectional water spreading. *ACS Appl Mater Interfaces*. 2017;9:5645–52.

[14] Barraza B, Olate-Moya F, Montecinos G, Ortega JH, Rosenkranz A, Tamburrino A, Palza H. Superhydrophobic SLA 3D printed materials modified with nanoparticles biomimicking the hierarchical structure of a rice leaf. *Sci Technol Adv Mater.* 2022;23:300–21.

[15] Yunusa M, Ozturk FE, Yildirim A, Tuvshindorj U, Kanik M, Bayindir M. Bio-inspired hierarchically structured polymer fibers for anisotropic non-wetting surfaces. *RSC Adv.* 2017;7:15553–60.

[16] Yong JL, Yang Q, Chen F, Zhang DS, Farooq U, Du GQ, Hou X. A simple way to achieve superhydrophobicity, controllable water adhesion, anisotropic sliding, and anisotropic wetting based on femtosecond-laser-induced line-patterned surfaces. *J Mater Chem A*. 2014;2:5499–507.

[17] Chung JY, Youngblood JP, Stafford CM. Anisotropic wetting on tunable micro-wrinkled surfaces. *J Soft Matter*. 2007;3:1163–9.

[18] Huang JH, Xu XT, Li SN, Peng LF, Lai XM. An experimental study on a rapid micro imprinting process. *J Mater Proc Technol*. 2020;283.

[19] Shen ZB, Zhang L, Li P, Liu HX, Liu K, Lin XY, et al. Altering the surface wettability of copper sheet using overlapping laser shock imprinting. *Appl Surf Sci.* 2021;543.

[20] Jin SY, Wang YX, Motlag M, Gao SJ, Xu J, Nian Q, et al. Large-area direct laser-shock imprinting of a 3D biomimic hierarchical metal surface for triboelectric nanogenerators. *Adv Mater.* 2018;30.

[21] Man JX, Zhao JY, Yang HF, Song LC, Liu D. Study on laser shock imprinting nanoscale line textures on metallic foil and its application in nanotribology. *Mater Design*. 2020;193.

[22] Yang HF, Jia L, Liu K, Wang Y, Xiong F, Liu H, Hao JB. High precision complete forming process of metal microstructure induced by laser shock imprinting. *Int J Adv Manufact Technol*. 2020;108:143–55.

[23] Choi DC, Kim HS. Performance evaluation of laser shock micro-patterning process on aluminum surface with various process parameters and loading schemes. *Opt Lasers \Eng*. 2020;124.

[24] Zhang BC, Yang HF, Xiong F, Liu H, Hao JB, Liu XH. Research on the transient forming process and high-temperature stability mechanism of warm laser shock imprinting. *Opt Lasers Eng*. 2021;146.

[25] Man JX, Yang HF, Wang YF, Chen HX, Xiong F. Study on controllable surface morphology of the micro-pattern fabricated on metallic foil by laser shock imprinting. *Opt Laser Technol*. 2019;119.

[26] Riedel M, Eichner A, Jetter R. Slippery surfaces of carnivorous plants: composition of epicuticular wax crystals in *Nepenthes alata* Blanco pitchers. *Planta*. 2003;218:87–97.

[27] Zhang WW, Yao YL. Micro scale laser shock processing of metallic components. *J Manufact Sci Eng—Trans ASME*. 2002;124:369–78.

[28] Wang SL, Yu NZ, Wang TQ, Ge P, Ye SS, Xue PH, et al. Morphology-patterned anisotropic Wetting surface for fluid control and gas–liquid separation in microfluidics. *ACS Appl Mater Interfaces*. 2016;8:13094–103.

[29] Jing X, Si WF, Sun J, Zhou JK, Lin JQ, Yu BJ, Lu MM. Wettability and droplet directional spread investigation of Crescent array surface inspired by slippery zone of *Nepenthes*. *Adv Mater Interfaces*. 2022;9.

[30] Wang LX, Yin K, Deng QW, Huang QQ, He J, Duan JA. Wetting ridge-guided directional water self-transport. *Adv Sci.* 2022;9.

Received 2023-10-11
Accepted 2024-01-09